

PAPER

Sensor fault diagnosis for uncertain dissimilar redundant actuation system of more electric aircraft via bond graph and improved principal component analysis

To cite this article: Ming Yu *et al* 2023 *Meas. Sci. Technol.* **34** 015120

View the [article online](#) for updates and enhancements.

You may also like

- [Finite Crystallization and Wulff shape emergence for ionic compounds in the square lattice](#)

Manuel Friedrich and Leonard Kreutz

- [MIL-Standards Verification of Battery Control for More Electric Aircraft Application](#)

Antonio Russo, Giacomo Canciello and Alberto Cavallo

- [Coupled Simulation of Electric Flight Dynamics and Physics Based Battery Model for Electric Aircraft Battery Pack Sizing Analysis](#)

Suryanarayana Kolluri, Krishna Shah, Mengyuan Wang et al.

Breath Biopsy[®] OMNI[®]

The most advanced, complete solution for global breath biomarker analysis

BREATH[®]
BIOPSY

TRANSFORM YOUR
RESEARCH WORKFLOW



Expert Study Design
& Management



Robust Breath
Collection



Reliable Sample
Processing & Analysis



In-depth Data
Analysis



Specialist Data
Interpretation

Sensor fault diagnosis for uncertain dissimilar redundant actuation system of more electric aircraft via bond graph and improved principal component analysis

Ming Yu^{1,*} , Jie Meng¹, Rensheng Zhu², Wuhua Jiang³ and Qiang Shen⁴

¹ School of Electrical Engineering and Automation, Hefei University of Technology, Hefei 230009, People's Republic of China

² School of Mechanical Engineering, Hefei University of Technology, Hefei 230009, People's Republic of China

³ School of Automobile and Transportation Engineering, Hefei University of Technology, Hefei 230009, People's Republic of China

⁴ School of Aeronautics and Astronautics, Shanghai Jiao Tong University, Shanghai 200240, People's Republic of China

E-mail: yu0202@hfut.edu.cn

Received 11 January 2022, revised 5 May 2022

Accepted for publication 3 October 2022

Published 26 October 2022



Abstract

This paper develops a sensor condition monitoring method integrating the model-based bond graph (BG) technique and data-driven principal component analysis (PCA) for the dissimilar redundant actuation system of more electric aircraft with uncertain parameters. The uncertain dissimilar redundant actuation system is modeled by BG in linear fractional transformation form. After that, the analytical redundancy relations containing the nominal part and the uncertain part can be derived, based on which the adaptive thresholds and the fault signature matrix (FSM) can be obtained for robust fault detection and fault isolation. To improve the fault isolation performance under the multiple faults condition, a new fault isolation method integrating FSM and improved PCA (IPCA) is developed, where the possible fault set generated from the FSM is further refined by the IPCA module with an improved reconstruction algorithm and cyclic PCA monitoring model to achieve a more efficient fault isolation result. The effectiveness of the proposed approach is validated by simulation investigations.

Keywords: uncertain dissimilar redundant actuation system, bond graph, analytical redundancy relations, fault signature matrix, improved principal component analysis

(Some figures may appear in colour only in the online journal)

* Author to whom any correspondence should be addressed.

1. Introduction

With the emergence of more electric aircraft, the dissimilar redundant actuation system composed of a servo-controlled hydraulic actuator (SHA) and an electromechanical actuator (EMA) is widely used in the aviation field [1]. However, compared with the traditional actuation system, the dissimilar redundant system has a more complex structure and is prone to failure [2]. In order to ensure the safety and reliability of the system, many sensors are used to monitor the health conditions. Sensors undertake the task of data acquisition and their performance usually has a significant impact on the system control performance [3]. Thus, it is demanding to develop a sophisticated and reliable sensor fault detection and isolation (FDI) method for the dissimilar redundant actuation system of more electric aircraft.

Generally speaking, the sensor FDI approaches can be classified into two types, i.e. the data-driven approach and the model-based approach. The data-driven approach relies on sensor measurements to extract the feature for fault detection. Since it does not require the building of precise physical or mathematical models of the system under monitoring, great flexibility can be expected, which makes this approach popular in the field of FDI [4–8]. Principal component analysis (PCA) is a commonly used data-driven FDI method for sensor condition monitoring [4]. Many studies show that PCA can achieve attractive FDI performance. A PCA-based FDI method is introduced in [5] for rolling bearing systems. In [6], the FDI method with PCA through data-processing is developed for a nuclear power plant where false alarms can be reduced. In [7], a fractal-based dynamic kernel PCA method is proposed to address the weakness of the classical dynamic kernel PCA method in determining the number of principal components. An improved PCA (IPCA) for multiple faults isolation is developed in [8]. However, since PCA is the lack of ability to determine the possible faulty sensors in advance, the isolation procedure requires the simultaneous monitoring of all sensors in the system which could lead to daunting computational cost.

Unlike the data-driven approach, the model-based approach utilizes a precise physical or mathematical model which can capture the dynamic characteristics of the system to obtain relatively accurate diagnostic results [9–12]. Among the various modeling approaches, the bond graph (BG) is an effective tool for modeling the complex continuous system across multiple energy domains [13–16]. In [13], a BG model-based fault diagnosis method is proposed for the steer-by-wire system. In this work, a new fault isolation method based on the fine state machine is developed by combining dependent and independent analytical redundancy relationships (ARRs) where the fault isolation ability is improved. A cuckoo search-particle filter is proposed to achieve fault identification. However, the influence of parameter uncertainty is ignored in this work. In [14], an improved fault diagnosis method based on

sensitivity signature is proposed for hybrid systems, where the sensitivity signature is composed of three signs. Compared with the traditional binary signature, the sensitivity signature generates more distinguished signatures to improve the ability of fault isolation under a single fault condition. However, due to uncertain eliminating effects, this method may not function well under a multiple faults condition. In [15], a hybrid condition monitoring method based on the bicausal-BG model and extreme learning machine is developed for the nonlinear mechatronic system where the performance of fault isolation is improved. However, this work only considers the single fault scenario. In [16], a decentralized FDI method based on diagnostic BG and PCA is developed for large-scale systems. In this method, the residuals generated from the diagnostic BG model with a decentralized architecture are employed to detect which subsystem is faulty. To further determine the true fault, a strongly isolating incidence matrix is designed for the subsystem, and the structured residuals are generated through PCA. However, the strongly isolating incidence matrix is only effective for the single fault condition.

In order to solve the aforementioned problems, a new sensor condition monitoring approach via the uncertain BG (UBG) model and IPCA is developed for the dissimilar redundant actuation system of more electric aircraft in the presence of multiple sensor faults. The developed method is denoted as UBG-IPCA. The main advantage of the developed method in this paper over the method in [16] lies in the fact that the developed method can effectively address the problem of multiple faults isolation by a cyclic PCA monitoring model and an improved reconstruction algorithm (IRA). The dissimilar redundant actuation system is modeled by UBG, based on which the ARRs incorporating the nominal part and uncertain part can be derived. The adaptive thresholds are obtained from the uncertain part of ARRs to detect the faults under parameter uncertainties. The fault signature matrix (FSM) is constructed according to the nominal part of ARRs to isolate the possible fault set (PFS). In order to refine the PFS, the IPCA module with IRA and cyclic PCA monitoring model is employed to determine the true faults. The main contribution of this work lies in the development of a new fault isolation method based on UBG-IPCA for the uncertain dissimilar redundant actuation system of more electric aircraft, which can simultaneously improve the performance of multiple faults isolation and reduce the computational cost of PCA. The advantage of UBG-IPCA over the fault isolation aided by fault estimation developed in [17] is that the UBG-IPCA does not require prior information on the fault type (e.g. bias fault and drift fault).

The rest of this paper is organized as follows. Section 2 builds the UBG model of the dissimilar redundant actuation system. In section 3, the developed FDI approach based on UBG-IPCA is introduced. In section 4, simulation results are analyzed in detail. Finally, section 5 concludes the paper.

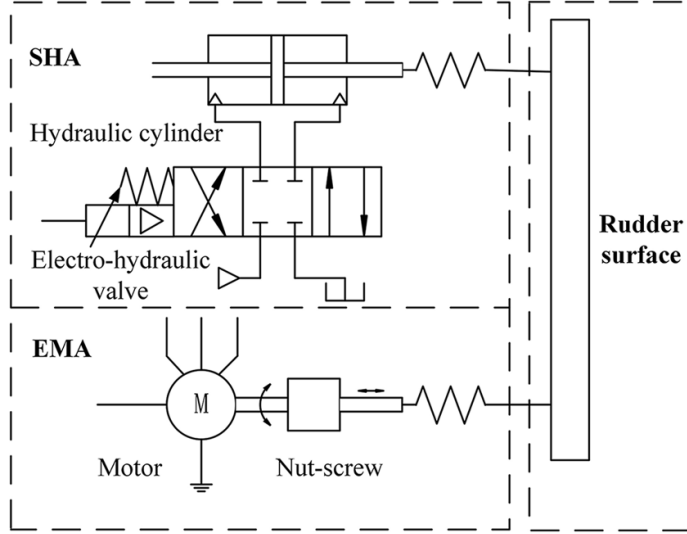


Figure 1. Dissimilar redundant actuation system of more electric aircraft.

2. UBG model of dissimilar redundant actuation system

BG is a graphical modeling method based on energy conservation law for continuous systems with multiple energy domains. In BG, generic elements employed to describe the physical system mainly include resistance element R , capacitance element C , inertia element I , junction elements 0 and 1, transformer elements TF and GY , and source elements Se and Sf . The bonds, defined as two power variables (i.e. effort e and flow f), are used to connect the generic elements and capture the power exchange between different elements. At the end of every bond, a vertical stroke is designed to describe the causality between power variables [18]. Once the causalities of all bonds are determined, the constitutive relationships of BG elements characterizing the element behaviors can be systematically derived.

As shown in figure 1, the dissimilar redundant actuation system of more electric aircraft mainly consists of three subsystems: the SHA subsystem, the EMA subsystem and the rudder surface subsystem. The SHA subsystem is composed of an electro-hydraulic valve and a hydraulic cylinder. The EMA subsystem consists of a motor and a nut-screw. The forces generated by the SHA and EMA act together on the rudder surface to drive the load.

To model the dissimilar redundant actuation system of more electric aircraft with parameter uncertainty, the UBG model in linear fractional transformation form is utilized [19]. The multiplicative uncertainty of BG element $i \in \{R, I, C\}$ is denoted by δ_i . The fictive effort and flow inputs (i.e. MSe and MSf) represent the additional effort and flow modulated by δ_i , respectively. The De^* and Df^* denote the virtual sensors instead of the true measurement. The UBG of the dissimilar redundant actuation system is

shown in figure 2, and can be divided into six parts as follows.

- (a) Motor. The electrical part of the motor is modeled by resistance element $R : R_w$ where R_w is stator resistance, inertia element $I : L_w$ where L_w is stator inductance. The uncertainties of resistance element $R : R_w$ and inertia element $I : L_w$ are denoted by δ_{R_w} and δ_{L_w} , respectively. The current generated in the motor electrical part is converted into torque in the mechanical part of the motor through gyrator element $GY : K_m$ where K_m is the current-to-torque constant. The mechanical part of the motor is characterized by inertia element $I : J_m$ where J_m is rotor inertia, resistance element $R : f_m$ where f_m is the viscous friction coefficient of motor, and effort source Se which represents the starting friction torque of the motor rotor. The uncertainties of inertia element $I : J_m$ and resistance element $R : f_m$ are denoted by δ_{J_m} and δ_{f_m} , respectively.
- (b) Nut-screw. The nut-screw is modeled by transformer element $TF : p$ where p is the lead of screw, resistance element $R : f_r$ where f_r is viscous friction coefficient of nut-screw, capacitance element $C : K_s$ where K_s is nut-screw stiffness, inertia element $I : m$ where m is rod mass, and capacitance element $C : K_1$ where K_1 is the stiffness of shaft connecting nut-screw and rudder surface. The uncertainties of resistance element $R : f_r$, capacitance element $C : K_s$, inertia element $I : m$, and capacitance element $C : K_1$ are denoted by δ_f , δ_{1/K_s} , δ_m , and δ_{1/K_1} , respectively.
- (c) Electro-hydraulic valve. The electro-hydraulic valve is modeled by resistance element $R : K_c$ where K_c is the pressure gain of the servo valve, flow source $Sf : K_q x_v$ where K_q and x_v represent current gain and output displacement

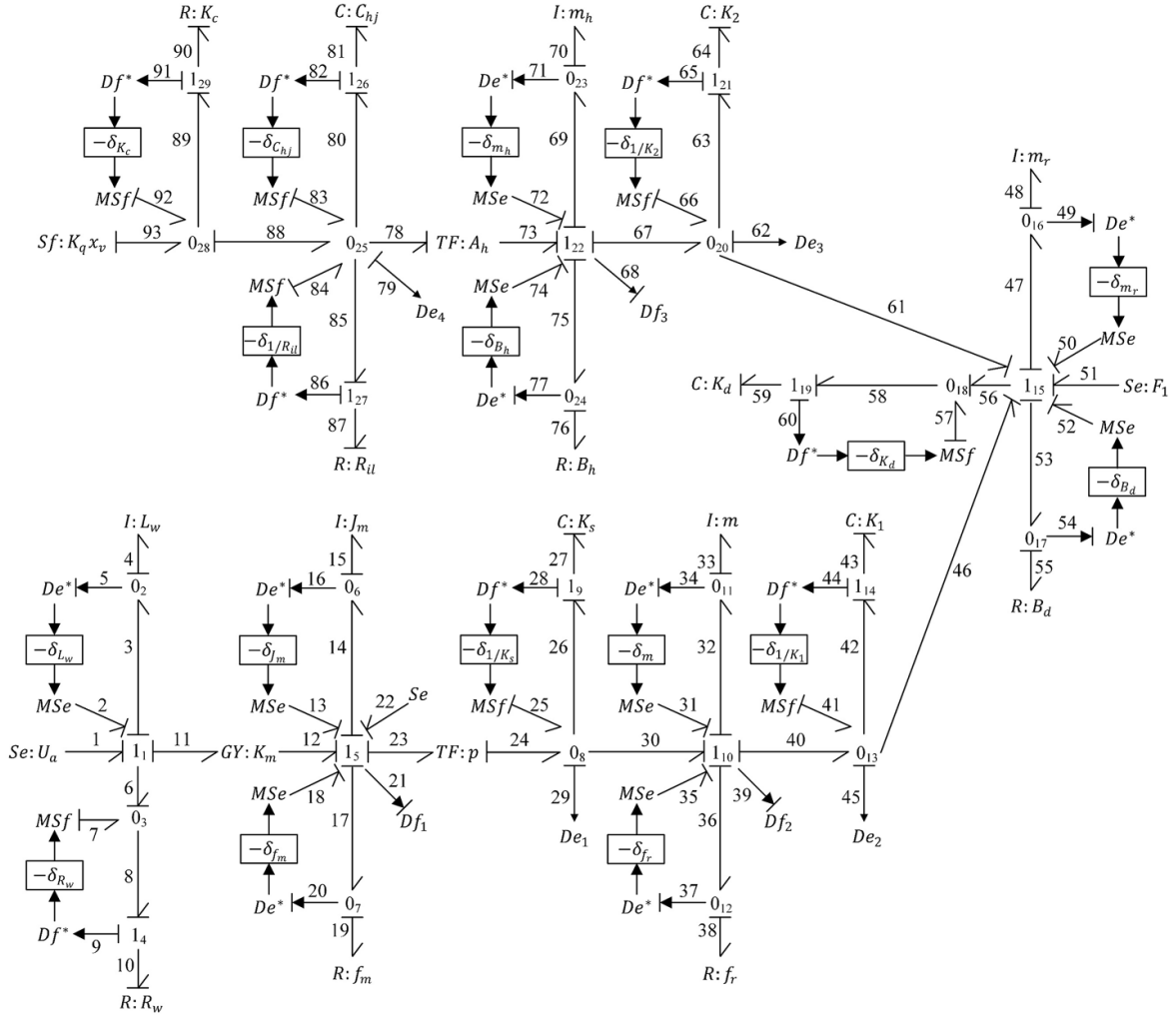


Figure 2. UBG model of dissimilar redundant actuation system.

of the servo valve, respectively. The uncertainty of resistance element $R : K_c$ is denoted by δ_{K_c} .

(d) Hydraulic cylinder. The hydraulic cylinder is modeled by capacitance element $C : C_{hj}$ where C_{hj} is the capacitance effect of the hydraulic cylinder, and resistance element $R : R_{il}$ where R_{il} is the internal leakage coefficient. The uncertainties of capacitance element $C : C_{hj}$ and resistance element $R : R_{il}$ are denoted by $\delta_{C_{hj}}$ and $\delta_{1/R_{il}}$, respectively.

(e) Piston. The piston is modeled by transformer element $TF : A_h$ where A_h is the piston effective area, resistance element $R : B_h$ where B_h is the viscous friction coefficient of the piston, inertia element $I : m_h$ where m_h is the mass of the piston, and capacitance element $C : K_2$ where K_2 is the stiffness of the shaft connecting piston rod and rudder surface. The uncertainties of resistance element $R : B_h$, inertia element $I : m_h$, and capacitance element $C : K_2$ are denoted by δ_{B_h} , δ_{m_h} , and δ_{1/K_2} , respectively.

(f) Rudder surface load. The rudder surface load is modeled by effort source $Se : F_1$ where F_1 is loading force of rudder surface, inertia element $I : m_r$ where m_r is rudder surface

mass, and capacitance element $C : K_d$ where K_d is stable load proportional coefficient of rudder surface. The uncertainties of inertia element $I : m_r$ and capacitance element $C : K_d$ are denoted by δ_{m_r} and δ_{K_d} , respectively.

There are seven sensors $\{Df_1, De_1, Df_2, De_2, Df_3, De_3, Df_4\}$ used to measure the motor angular velocity, the elastic force of the nut-screw, the rod velocity of the nut-screw, the force between the nut-screw and the rudder surface, the force between the piston rod and the rudder surface, the rod velocity of the piston, and the pressure difference in the hydraulic cylinder chamber, respectively.

From the UBG model, seven independent ARRs can be derived in equation (1) by inverting the causalities of the sensors [20]. Each ARR is composed of two separated parts, as shown in equations (2)–(8), where the nominal parts $r_1, r_2, r_3, r_4, r_5, r_6, r_7$ describe the operating states, and the uncertain parts $a_1, a_2, a_3, a_4, a_5, a_6, a_7$ represent the adaptive thresholds during normal conditions:

$$\left\{ \begin{array}{l} \text{ARR}_1 : r_1 - (w_{L_w} J_m + w_{J_m} L_w + w_{L_w} w_{J_m}) \frac{d^2 Df_1}{dt^2} \\ \quad - (w_{L_w} f_m + w_{f_m} L_w + w_{L_w} w_{f_m}) \frac{dDf_1}{dt} \\ \quad - (w_{R_w} J_m + w_{J_m} R_w + w_{R_w} w_{J_m}) \frac{dDf_1}{dt} \\ \quad - (w_{R_w} f_m + w_{f_m} R_w + w_{R_w} w_{f_m}) Df_1 \\ \quad - w_{L_w} \frac{p}{2\pi} \frac{dDe_1}{dt} - w_{R_w} \left(\frac{p}{2\pi} De_1 - S_e \right) = 0 \\ \text{ARR}_2 : r_2 + w_{1/K_s} = 0 \\ \text{ARR}_3 : r_3 + w_m + w_{f_r} = 0 \\ \text{ARR}_4 : r_4 - \left(w_{K_d} \frac{1}{K_1} + w_{1/K_1} K_d + w_{K_d} w_{1/K_1} \right) \frac{dDe_2}{dt} \\ \quad - \left(w_{m_r} \frac{1}{K_1} + w_{1/K_1} m_r + w_{1/K_1} w_{m_r} \right) \frac{d^3 De_2}{dt^3} \\ \quad - \left(w_{B_d} \frac{1}{K_1} + w_{1/K_1} B_d + w_{1/K_1} w_{B_d} \right) \frac{d^2 De_2}{dt^2} \\ \quad + w_{m_r} \frac{d^2 Df_2}{dt^2} + w_{B_d} \frac{dDf_2}{dt} + w_{K_d} Df_2 = 0 \end{array} \right. \quad (1)$$

$$\left. \begin{array}{l} \text{ARR}_5 : r_5 - \left(w_{K_d} \frac{1}{K_2} + w_{1/K_2} K_d + w_{K_d} w_{1/K_2} \right) \frac{dDe_3}{dt} \\ \quad - \left(w_{m_r} \frac{1}{K_2} + w_{1/K_2} m_r + w_{1/K_2} w_{m_r} \right) \frac{d^3 De_3}{dt^3} \\ \quad - \left(w_{B_d} \frac{1}{K_2} + w_{1/K_2} B_d + w_{1/K_2} w_{B_d} \right) \frac{d^2 De_3}{dt^2} \\ \quad + w_{m_r} \frac{d^2 Df_3}{dt^2} + w_{B_d} \frac{dDf_3}{dt} + w_{K_d} Df_3 = 0 \end{array} \right.$$

$$\text{ARR}_6 : r_6 + w_{m_h} + w_{B_h} = 0$$

$$\left. \text{ARR}_7 : r_7 + w_{K_c} + w_{1/R_{il}} + w_{C_{bj}} = 0 \right.$$

$$\left\{ \begin{array}{l} r_1 = L_w J_m \frac{d^2 Df_1}{dt^2} + (L_w f_m + R_w J_m) \frac{dDf_1}{dt} \\ \quad + (R_w f_m + K_m^2) Df_1 + L_w \frac{p}{2\pi} \frac{dDe_1}{dt} \\ \quad + R_w \left(\frac{p}{2\pi} De_1 - S_e \right) - K_m U_a \\ a_1 = (|w_{L_w}| J_m + |w_{J_m}| L_w + |w_{L_w} w_{J_m}|) \frac{d^2 Df_1}{dt^2} \\ \quad + (|w_{L_w}| f_m + |w_{f_m}| L_w + |w_{L_w} w_{f_m}|) \frac{dDf_1}{dt} \\ \quad + (|w_{R_w}| J_m + |w_{J_m}| R_w + |w_{R_w} w_{J_m}|) \frac{dDf_1}{dt} \\ \quad + (|w_{R_w}| f_m + |w_{f_m}| R_w + |w_{R_w} w_{f_m}|) Df_1 \\ \quad + |w_{L_w}| \frac{p}{2\pi} \frac{dDe_1}{dt} + |w_{R_w}| \left(\frac{p}{2\pi} De_1 - S_e \right) \end{array} \right. \quad (2)$$

$$\left\{ \begin{array}{l} r_2 = \frac{p}{2\pi} Df_1 - \frac{1}{K_s} \frac{dDe_1}{dt} - Df_2 \\ a_2 = |w_{1/K_s}| \end{array} \right. \quad (3)$$

$$\left\{ \begin{array}{l} r_3 = De_1 - De_2 - m \frac{dDf_2}{dt} - f_r Df_2 \\ a_3 = |w_m| + |w_{f_r}| \end{array} \right. \quad (4)$$

$$\left\{ \begin{array}{l} r_4 = \left(1 + \frac{K_d}{K_1} \right) \frac{dDe_2}{dt} + \frac{dDe_3}{dt} - m_r \frac{d^2 \left(Df_2 - \frac{1}{K_1} \frac{dDe_2}{dt} \right)}{dt^2} \\ \quad - B_d \frac{d \left(Df_2 - \frac{1}{K_1} \frac{dDe_2}{dt} \right)}{dt} + \frac{dF_1}{dt} - K_d Df_2 \\ a_4 = \left(|w_{K_d}| \frac{1}{K_1} + |w_{1/K_1}| K_d + |w_{K_d} w_{1/K_1}| \right) \frac{dDe_2}{dt} \\ \quad + \left(|w_{m_r}| \frac{1}{K_1} + |w_{1/K_1}| m_r + |w_{m_r} w_{1/K_1}| \right) \frac{d^3 De_2}{dt^3} \\ \quad + \left(|w_{B_d}| \frac{1}{K_1} + |w_{1/K_1}| B_d + |w_{B_d} w_{1/K_1}| \right) \frac{d^2 De_2}{dt^2} \\ \quad + |w_{m_r}| \frac{d^2 Df_2}{dt^2} + |w_{B_d}| \frac{dDf_2}{dt} + |w_{K_d}| Df_2 \end{array} \right. \quad (5)$$

$$\left\{ \begin{array}{l} r_5 = \left(1 + \frac{K_d}{K_2} \right) \frac{dDe_3}{dt} + \frac{dDe_2}{dt} - m_r \frac{d^2 \left(Df_3 - \frac{1}{K_2} \frac{dDe_3}{dt} \right)}{dt^2} \\ \quad - B_d \frac{d \left(Df_3 - \frac{1}{K_2} \frac{dDe_3}{dt} \right)}{dt} + \frac{dF_1}{dt} - K_d Df_3 \\ a_5 = \left(|w_{K_d}| \frac{1}{K_2} + |w_{1/K_2}| K_d + |w_{K_d} w_{1/K_2}| \right) \frac{dDe_3}{dt} \\ \quad + \left(|w_{m_r}| \frac{1}{K_2} + |w_{1/K_2}| m_r + |w_{m_r} w_{1/K_2}| \right) \frac{d^3 De_3}{dt^3} \\ \quad + \left(|w_{B_d}| \frac{1}{K_2} + |w_{1/K_2}| B_d + |w_{B_d} w_{1/K_2}| \right) \frac{d^2 De_3}{dt^2} \\ \quad + |w_{m_r}| \frac{d^2 Df_3}{dt^2} + |w_{B_d}| \frac{dDf_3}{dt} + |w_{K_d}| Df_3 \end{array} \right. \quad (6)$$

$$\left\{ \begin{array}{l} r_6 = A_h De_4 - m_h \frac{dDf_3}{dt} - B_h Df_3 - De_3 \\ a_6 = |w_{m_h}| + |w_{B_h}| \end{array} \right. \quad (7)$$

$$\left\{ \begin{array}{l} r_7 = K_q x_v - \left(K_c + \frac{1}{R_{il}} \right) De_4 - C_{bj} \frac{dDe_4}{dt} - A_h Df_3 \\ a_7 = |w_{K_c}| + |w_{1/R_{il}}| + |w_{C_{bj}}| \end{array} \right. \quad (8)$$

with

$$\begin{aligned}
 w_{L_w} - \delta_{L_w} L_w, \quad w_{f_m} = -\delta_{f_m} f_m, \quad w_{R_w} = -\delta_{R_w} R_w \\
 w_{J_m} - \delta_{J_m} J_m, \quad w_{1/K_s} = -\delta_{1/K_s} \frac{1}{K_s} \frac{dDe_1}{dt}, \quad w_m = -\delta_m m \frac{dDf_2}{dt} \\
 w_{f_r} - \delta_{f_r} f_r Df_2, \quad w_{K_c} = -\delta_{K_c} K_c De_4, \quad w_{1/K_1} = -\delta_{1/K_1} \frac{1}{K_1} \\
 w_{B_d} = -\delta_{B_d} B_d, \quad w_{K_d} = -\delta_{K_d} K_d, \quad w_{1/K_2} = -\delta_{1/K_2} \frac{1}{K_2} \\
 w_{m_h} = -\delta_{m_h} m_h \frac{dDf_3}{dt}, \quad w_{B_h} = -\delta_{B_h} B_h Df_3, \quad w_{m_r} = -\delta_{m_r} m_r \\
 w_{1/R_{il}} = -\delta_{\frac{1}{R_{il}}} \frac{1}{R_{il}} De_4, \quad w_{C_{hj}} = -\delta_{C_{hj}} C_{hj} \frac{dDe_4}{dt}.
 \end{aligned}$$

3. FDI based on UBG-IPCA

In general, the FDI procedure consists of two tasks: fault detection and fault isolation. Fault detection can be carried out through comparing the residuals (i.e. the numerical values of ARRs) with their corresponding adaptive thresholds, and a fault condition is indicated when any of the residuals surpass their thresholds. To describe the consistency of residuals, a binary coherence vector $CV = [cv_1, cv_2, \dots, cv_7]$ is defined, where $cv_i = 0$ ($i = 1, 2, \dots, 7$) represents that ARR_i is consistent (i.e. i th residual is within its adaptive threshold), and 1 otherwise [20]. During the system monitoring, a fault condition is declared if the CV is nonzero, and zero otherwise.

Once a fault is detected, the next task is to implement the fault isolation procedure to obtain PFS which could account for the observed fault symptom. The PFS is generated by comparing the observed nonzero CV with the FSM established from the nominal parts of ARRs. Table 1 gives the FSM of the dissimilar redundant actuation system. In this table, the D_b represents the detectability, where $D_b = 1$ represents the fault in the corresponding row being detectable, and 0 otherwise. It can be observed from the table that all sensor faults can be detected. As for fault isolability, the situation is complicated under the multiple faults condition since different combinations of faults may match the same nonzero CV. For example, if the observed CV is $[1 \ 1 \ 1 \ 0 \ 0 \ 0 \ 0]$, the PFS is $\{Df_1 \& De_1, De_1\}$. In this condition, no one can determine whether Df_1 is faulty or not because its fault signature is covered by the one of De_1 . To deal with the limited multiple faults isolation ability of FSM, the UBG-IPCA method is developed. PCA is a method that can reduce the dimensions of variables and transform a set of correlated variables into a set of new uncorrelated variables. The variables of the dissimilar redundant actuation system are multi-dimensional and have a certain correlation. Thus, desirable performance can be expected by employing PCA for sensor fault isolation. Note that the main work of this paper is to develop a new cyclic monitoring model based on FSM and fault reconstruction to realize multiple sensor faults isolation. As a data dimensionality reduction method, PCA is not the only choice. The main reason for using PCA to realize

Table 1. FSM of dissimilar redundant actuation system.

	ARR ₁	ARR ₂	ARR ₃	ARR ₄	ARR ₅	ARR ₆	ARR ₇	D_b
Df_1	1	1	0	0	0	0	0	1
De_1	1	1	1	0	0	0	0	1
Df_2	0	1	1	1	0	0	0	1
De_2	0	0	1	1	1	0	0	1
De_3	0	0	0	1	1	1	0	1
Df_3	0	0	0	0	1	1	1	1
De_4	0	0	0	0	0	1	1	1

sensor fault isolation is that PCA is the most commonly used data-driven method in the field of sensor FDI due to its simplicity and good performance of dimensionality reduction. The IPCA, which can effectively address the fault leakage problem of the traditional PCA model under the multiple faults condition, mainly includes two parts: the PCA monitoring module and the fault reconstruction module.

In the PCA monitoring module, X is defined as a standardized training data matrix with m variables and n samples. Its covariance matrix R is given in equation (9). By decomposing the covariance matrix R , the eigenvalues $\lambda_1 \geq \lambda_2 \geq \dots \geq \lambda_m$ and corresponding eigenvectors p_1, p_2, \dots, p_m of X can be obtained:

$$R = \frac{X^T X}{m-1}. \quad (9)$$

There are two commonly used methods to determine the number of principal components k : cumulative percent variance (CPV) and cross validation based on the prediction error of square sum [21]. The CPV method is selected to calculate k where the CPV is defined as:

$$CPV = \frac{\sum_{i=1}^{i=k} \lambda_i}{\sum_{i=1}^{i=m} \lambda_i} \times 100\%. \quad (10)$$

After k is determined, the original data matrix X can be divided into two parts:

$$X = \hat{X} + \tilde{X} = \hat{C}X + \tilde{C}X \quad (11)$$

where $\hat{C} = \hat{P}\hat{P}^T$, $\tilde{C} = \tilde{P}\tilde{P}^T = I - \hat{C}$, $\hat{P} = \{p_1, p_2, \dots, p_k\}$ is the loading matrix, $\tilde{P} = \{p_{k+1}, p_{k+2}, \dots, p_m\}$ is the residual matrix, \hat{C} is the principal component space (PCS) that contains most variation information of the original data, and \tilde{C} is the residual space (RS) that contains most measurement noise and fault information.

Hotelling T^2 (T^2 statistics) and square prediction error (Q statistics) are two indices to describe the results of PCA monitoring [22], where T^2 statistics describe the amount of variation of measurement data in PCS, and Q statistics describe the total change amount in RS. To obtain more accurate monitoring results, both indices are employed to carry out

the PFS refinement task, and the PFS is refined (i.e. all true faults are determined) if the statistics are within their corresponding control limits.

The T^2 and Q statistics are defined as follows:

$$T^2 = x \hat{P} \Lambda_k^{-1} \hat{P}^T x \quad (12)$$

$$Q = e e^T \quad (13)$$

where x is the testing vector, $\Lambda_k^{-1} = \text{diag}(\lambda_1, \lambda_2, \dots, \lambda_k)$ is the diagonal matrix consisting of the first k eigenvalues, $e = x(I - \hat{P} \hat{P}^T)$ is the residual vector of x . The control limits of T^2 and Q statistics are given in equations (14) and (15):

$$T_{\text{UCL}}^2 = \frac{k(n^2 - 1)}{n(n - k)} F_{k, n-k; \alpha} \quad (14)$$

$$Q_{\text{UCL}} = \theta_1 \left(1 + \frac{c_\alpha \sqrt{2\theta_2 h_0^2}}{\theta_1} + \frac{\theta_2 h_0 (h_0 - 1)}{\theta_1^2} \right)^{\frac{1}{h_0}} \quad (15)$$

where $\theta_j = \sum_{i=k+1}^n \lambda_i^j$, ($j = 1, 2, 3$), $h_0 = 1 - \frac{2\theta_1\theta_3}{3\theta_2^2}$, $F_{k, n-k; \alpha}$ is the critical value of F distribution with freedoms k and $n - k$, α is the confidence level selected as 0.99 or 0.95. c_α represents a standardized normal distribution with $1 - \alpha$ confidence limit.

In the PCA monitoring module, the contributions of all possible faulty sensors in PFS to T^2 and Q statistics are compared. If sensor x_i shows the maximum contribution among all sensors, it can be considered as a faulty sensor. The contributions of sensor x_i to T^2 and Q statistics are defined as follows:

$$\text{CONT}_i^Q = \frac{\|x_i(I - \hat{P} \hat{P}^T)\|}{\|x(I - \hat{P} \hat{P}^T)\|} = \frac{e_i^2}{\sum_{i=1}^m e_i^2} \times 100\% \quad (16)$$

$$\text{CONT}_i^{T^2} = \sum_{j=1}^k T_{i,j}^2 = \sum_{j=1}^k \left(\frac{t_j p_{j,i}}{\lambda_j} x_i \right) (i = 1, 2, \dots, m) \quad (17)$$

where t_j is the j th element of the score vector of x , and $p_{j,i}$ is the i th element of the p_j eigenvector.

In the fault reconstruction module, the data of a faulty sensor are reconstructed once the faulty sensor is determined. Through the reconstruction algorithm, the fault data of the sensor can be recovered to the normal value to eliminate its fault characteristics. The general idea for the traditional iterative reconstruction algorithm (TRA) is to utilize an iterative approach to project the fault data onto the PCS of PCA model many times to obtain the best reconstruction value of the faulty sensor [23]. This method is simple and direct, but only considers the PCS and ignores the influence of noise and disturbance (i.e. RS) in original data. In the case of multiple faults, TRA cannot accurately reconstruct the data of all faulty sensors, and the reconstruction error is large. To obtain a better reconstruction result under the multiple faults condition, IRA is employed. The basic principle of IRA can be described as follows:

3.1. Reconstruction of PCS

According to equation (11), the projection value of the measurement data in the PCS can be expressed as:

$$\hat{X} = \begin{bmatrix} \hat{x}_1 \\ \hat{x}_2 \\ \vdots \\ \hat{x}_n \end{bmatrix} = \hat{C}X = \begin{bmatrix} \hat{C}_{1,1} & \hat{C}_{1,2} & \cdots & \hat{C}_{1,n} \\ \hat{C}_{2,1} & \ddots & \ddots & \vdots \\ \vdots & \ddots & \ddots & \vdots \\ \hat{C}_{n,1} & \cdots & \cdots & \hat{C}_{n,n} \end{bmatrix} \begin{bmatrix} x_1 \\ x_2 \\ \vdots \\ x_n \end{bmatrix}. \quad (18)$$

If a fault occurs in sensor x_i , its projection value \hat{x}_i in the PCS can be represented as:

$$\hat{x}_i = [\hat{C}_{i,1:(i-1)}, \hat{C}_{i,i}, \hat{C}_{i,(i+1):n}] [x_1, \dots, x_i, \dots, x_n] \quad (19)$$

where $\hat{C}_{i,i}$ is the element at the i th row and i th column of matrix \hat{C} , $\hat{C}_{i,1:(i-1)}$ and $\hat{C}_{i,(i+1):n}$ represent the elements from the first to the $(i-1)$ th column and the $(i+1)$ th to the last column in the i th row of matrix \hat{C} , respectively.

The measurement data of x_i can be divided into two parts:

$$\hat{x}_i = [\hat{C}_{i,1:(i-1)}, 0, \hat{C}_{i,(i+1):n}] X + \hat{C}_{i,i} x_i = \hat{C}^* X + \hat{C}_{i,i} x_i \quad (20)$$

where \hat{C}^* is the reconstructed PCS, $\hat{C}^* X$ is the projection value of the normal sensor in PCS, and $\hat{C}_{i,i} x_i$ is the projection value of the faulty sensor x_i in the PCS. The reconstruction of fault data is mainly carried out for $\hat{C}_{i,i} x_i$.

Since the PCS does not contain system noise and disturbance, the state of the previous instant can reflect the current state when the system is in a stable state. Thus, if the sensor x_i suffers fault at t , the fault data $x_i(t)$ can be corrected by the normal value of previous instant $x_i(t-1)$ and the other sensors without fault remain unchanged. The reconstruction value $\hat{x}_i^*(t)$ of sensor x_i in PCS at t can be defined as:

$$\hat{x}_i^*(t) = [\hat{C}_{i,1:(i-1)}, 0, \hat{C}_{i,(i+1):n}] X(t) + \hat{C}_{i,i} x_i(t-1). \quad (21)$$

3.2. Reconstruction of RS

Different from the PCS, the RS mainly contains the noise and disturbance information of the system, which has strong randomness and uncertainty. The RS at the previous instant $t-1$ cannot accurately reflect the noise and disturbance of current instant t . Thus, utilizing the projection value of measurement data in RS at the previous instant to represent the noise and disturbance of the current instant will lead to a larger reconstruction error. To improve the reconstruction accuracy of the algorithm, an average sliding window defined in equation (23) is used to select the samples, and the average projection value of samples in RS is calculated to replace the noise and disturbance of the current instant. The reconstruction value $\tilde{x}_i^*(t)$ of sensor x_i in RS at t can be expressed as:

$$\tilde{x}_i^*(t) = [\tilde{C}_{i,1:(i-1)}, 0, \tilde{C}_{i,(i+1):n}] X(t) + \tilde{C}_{i,i} \bar{x}_i(t) \quad (22)$$

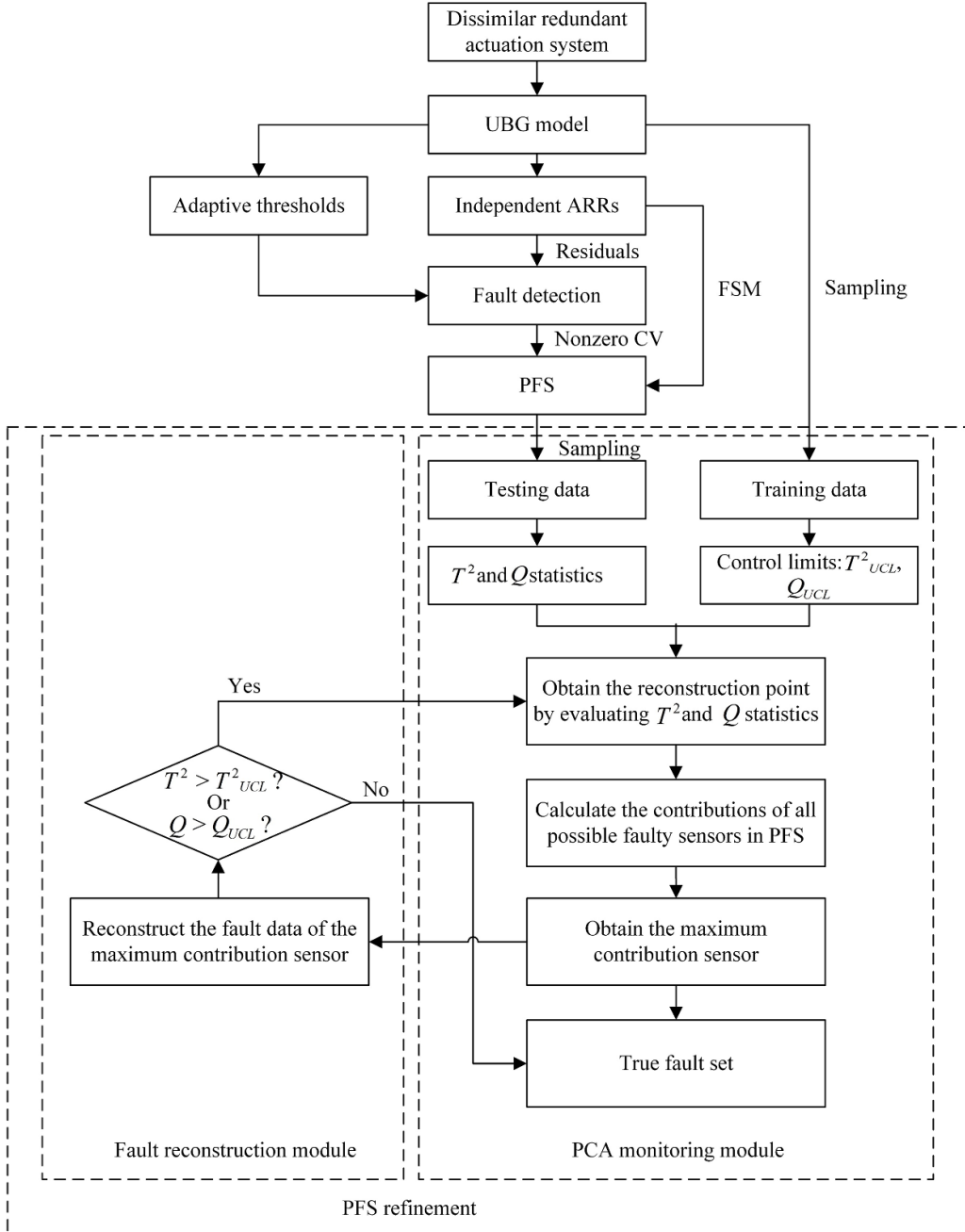


Figure 3. Complete framework of UBG-IPCA-based FDI.

$$\bar{x}_i(t) = \frac{1}{l} \sum_{j=t-l+1}^t x_i(j) \quad (23)$$

where l is the length of the sliding window.

The reconstruction value $\hat{x}_i^*(t)$ of x_i at t can be denoted as:

$$x_i^*(t) = \hat{x}_i^*(t) + \tilde{x}_i^*(t). \quad (24)$$

Figure 3 shows the framework of the developed UBG-IPCA method. In this method, the dissimilar redundant actuation system is modeled by the UBG technique. Then, the adaptive thresholds and the FSM are derived to detect the faults under parameter uncertainties and isolate the PFS. To determine the

true faults from the PFS, the possible faulty sensors will be further processed by the IPCA module. Through the PCA monitoring module, the faulty sensor can be determined by comparing the contributions of all possible faulty sensors in PFS. After that, the data of the faulty sensor are reconstructed by the fault reconstruction module. To determine if there are any other faults in the system, the reconstructed data are employed instead of the fault data for further monitoring. After several rounds of fault reconstruction and PCA monitoring, if the T^2 and Q statistics of all sensors in PFS fall below their control limits, it indicates that the data of all faulty sensors have been successfully reconstructed and the true faults are determined.

Table 2. Nominal parameter values of the dissimilar redundant actuation system.

Parameter	Value	Parameter	Value	Parameter	Value
L_w	0.0025 (H)	J_m	$0.0012 \text{ (kg m}^2)$	A_h	$1.47 \times 10^{-3} \text{ (m}^2)$
R_w	1.5 (\Omega)	f_m	$-4 \times 10^{-4} \text{ (Nms rad}^{-1})$	C_{hj}	$4.59 \times 10^{-14} \text{ (Pam}^{-3})$
K_m	$0.2 \text{ (Ns A}^{-1})$	K_q	$2.7 \text{ (m}^2 \text{ s}^{-1})$	B_h	$1 \times 10^4 \text{ (Nm s}^{-1})$
F_1	$-1 \times 10^4 \text{ (N)}$	B_d	$2300 \text{ (Nm s}^{-1})$	S_e	-0.01 (Nm)
f_r	$1 \times 10^4 \text{ (Nms rad}^{-1})$	K_s	$3 \times 10^8 \text{ (Nm}^{-1})$	m	1 (kg)
P	$2.54 \times 10^{-3} \text{ (m)}$	K_v	$1.52 \times 10^{-4} \text{ (mA}^{-1})$	K_c	$1.75 \times 10^{-11} \text{ (m}^3 \text{ s}^{-1} \text{ Pa}^{-1})$
R_{il}	$5 \times 10^{11} \text{ (Pam}^{-3} \text{ s}^{-1})$	m_h	55 (kg)	m_r	$1 \times 10^4 \text{ (Nms rad}^{-1})$

4. Simulations results

In order to evaluate the validity of the proposed FDI method based on UBG-IPCA for the dissimilar redundant actuation system of more electric aircraft, several tests are carried out in MATLAB/Simulink. The nominal parameter values of the dissimilar redundant actuation system are given in table 2 [24, 25]. The multiplicative uncertainty value of each parameter is set to 0.02. In simulation, random perturbations are given to the parameter values and these perturbations are kept within $\pm 2\%$ with respect to the nominal parameter values. For example, the nominal parameter value of R_w is 1.5Ω and its value is within $[1.5 - 0.02 \times 1.5, 1.5 + 0.02 \times 1.5] \Omega$ after perturbation. These perturbed parameters are put into the simulation model, by which the uncertain system can be established. The sampling period is set to 0.0001 s. The size of training data matrix X is 7×500 (i.e. 500 samples for each of the 7 sensors). The CPV is set to 90%. The control limits of T^2 and Q statistics are calculated with a confidence level of $\alpha = 99\%$. The length l of the sliding window is selected as 10.

The measurement equation of the i th sensor at instant t , i.e. $y_i(t)$, can be defined as follows:

$$y_i(t) = y_i^*(t) + f_i(t) + v_i(t) \quad (25)$$

where $y_i^*(t)$ is the normal measurement value, $f_i(t)$ is the measurement error caused by sensor fault, and $v_i(t)$ is the measurement noise.

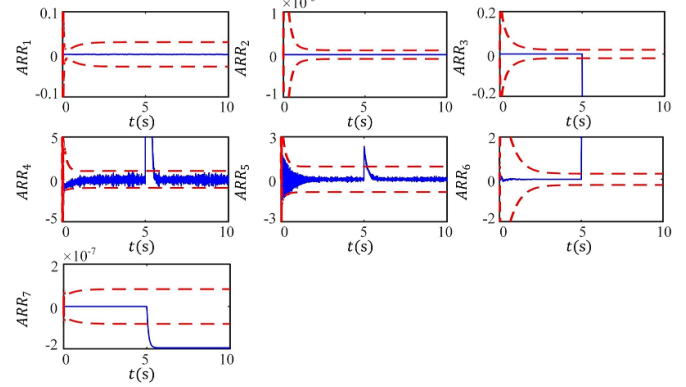
Here, the measurement noise is chosen as Gaussian noise with zero mean and 1×10^{-4} variance, i.e. $v_i(t) \sim N(0.1 \times 10^{-4})$. Bias fault and drift fault are two well-known sensor faults [26], and their fault characteristics are described in table 3, where t_0 represents the fault initiating instant, C_1 and C_2 represent the fault severities. For these two kinds of faults, three different fault scenarios are considered.

4.1. Scenario one: bias faults in sensors De_2 and De_4

For the first scenario, 1% and 0.2% bias faults are introduced in sensors De_2 and De_4 (i.e. $C_1 = 1\%$ for De_2 , $C_1 = 0.2\%$ for De_4) at 5 s (i.e. $t_0 = 5$ s), respectively. The residual responses are shown in figure 4, where the dashed lines represent the adaptive thresholds. It can be observed from the figure that ARR_3 , ARR_4 , ARR_5 , ARR_6 and ARR_7 exceed their corresponding thresholds at 5 s. Therefore, the CV is $[0 \ 0 \ 1 \ 1 \ 1 \ 1 \ 1]$. Comparing the CV with the FSM in table 1,

Table 3. Fault types of sensors.

Fault type	Fault characteristic
Bias fault	$f_i(t) = C_1 y_i^*(t_0)$
Drift fault	$f_i(t) = C_2 y_i^*(t_0) \arctan(t - t_0)$

**Figure 4.** Residual responses under the first scenario.

the PFS = $\{De_2 \& De_3 \& Df_3 \& De_4, De_2 \& De_4, De_2 \& Df_3 \& De_3, De_2 \& De_3 \& De_4\}$ is obtained. It is found that the true faults cannot be directly determined by FSM.

In order to refine the PFS, De_2 , De_3 , De_4 and Df_3 (i.e. possible faults which appear in PFS) are monitored by the IPCA module. The testing data are generated by sampling 500 data for each possible faulty sensor. After data processing, the T^2 and Q statistics are obtained. The T^2 and Q statistics are shown in figure 5, where the dashed lines represent control limits. It is observed that both statistics (i.e. T^2 and Q) exceed their corresponding control limits at the 200th sampling point. Figure 6 demonstrates the contributions of possible faulty sensors to T^2 and Q statistics, in which De_2 shows the maximum contribution among the monitored sensors. Since the maximum contribution sensor can be considered as a faulty sensor, De_2 is included in the true fault set.

To determine if there are other faults in PFS, the reconstruction process is conducted on De_2 to eliminate its fault characteristics, and then the reconstructed data of De_2 are utilized instead of the fault data for the subsequent monitoring. The data reconstruction results of De_2 are given in figure 7. For comparison, the TRA is adopted to reconstruct the fault data of De_2 under this fault scenario. It can be observed that the

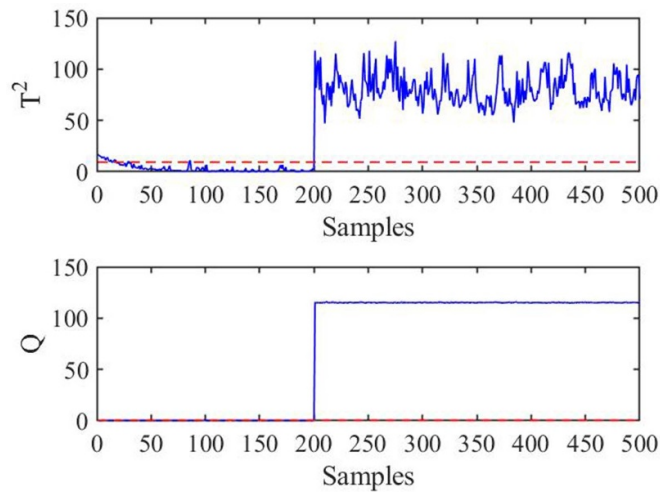


Figure 5. T^2 and Q statistics under the first scenario.

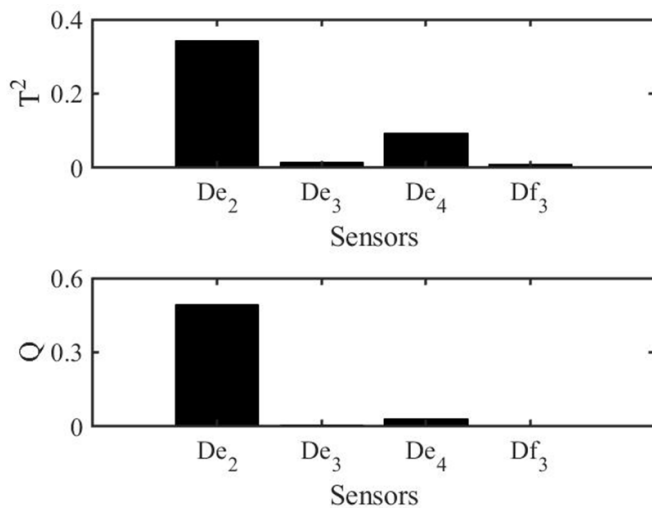


Figure 6. Contributions of possible faulty sensors to T^2 and Q statistics under the first scenario.

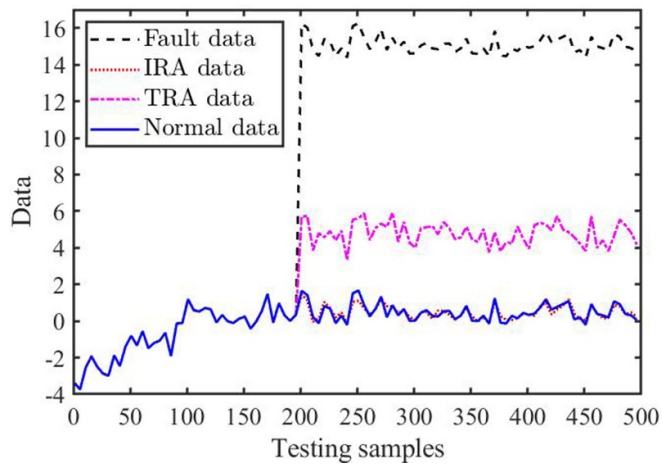
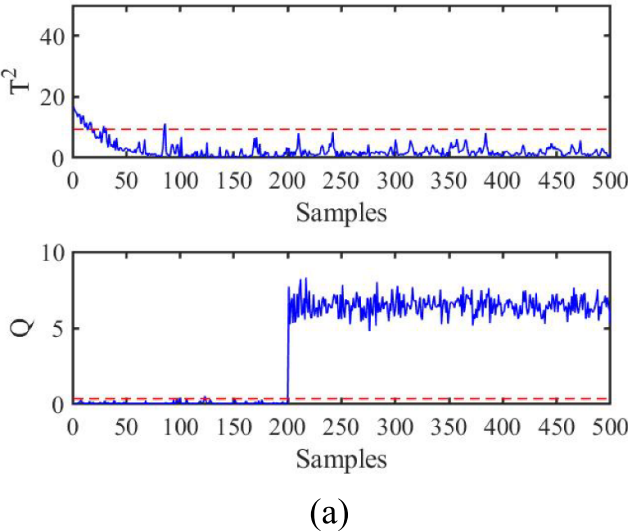
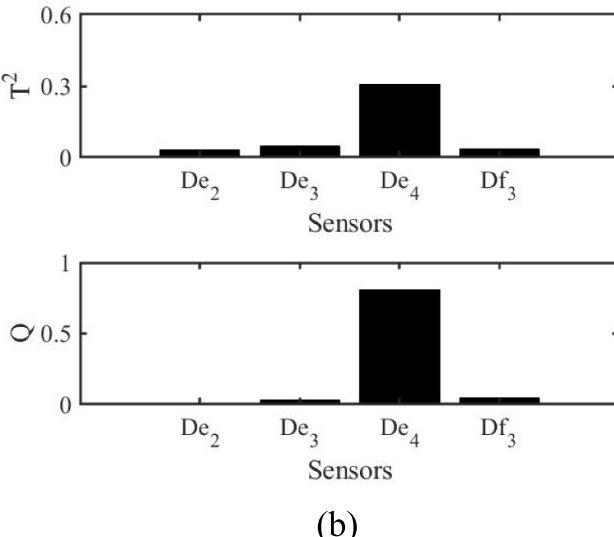


Figure 7. Reconstruction results of De_2 under the first scenario.



(a)



(b)

Figure 8. Results of second monitoring after reconstructing De_2 under the first scenario: (a) T^2 and Q statistics; (b) contributions of possible faulty sensors to T^2 and Q statistics.

IRA successfully reconstructs the fault data of De_2 (i.e. the reconstructed data of De_2 by using IRA are consistent with the normal values) under multiple faults condition, but the TRA cannot work well (i.e. the reconstructed data of De_2 by using TRA are inconsistent with the normal values). The IRA is superior to the TRA due to the fact that the IRA further considers the fault reconstruction of RS. After the fault data of De_4 are successfully reconstructed by IRA, the second monitoring process is activated. The results of the second monitoring are shown in figure 8. From the figure, it is found that Q statistics exceed the control limit at the 200th sampling point and the faulty sensor De_4 is determined. Thus, De_4 is added to the true fault set. Figure 9 shows the reconstruction results of De_4 based on IRA and TRA. Similarly, it can be found that the reconstruction performance of IRA is better than that of TRA. After the fault data of De_4 are reconstructed by IRA,

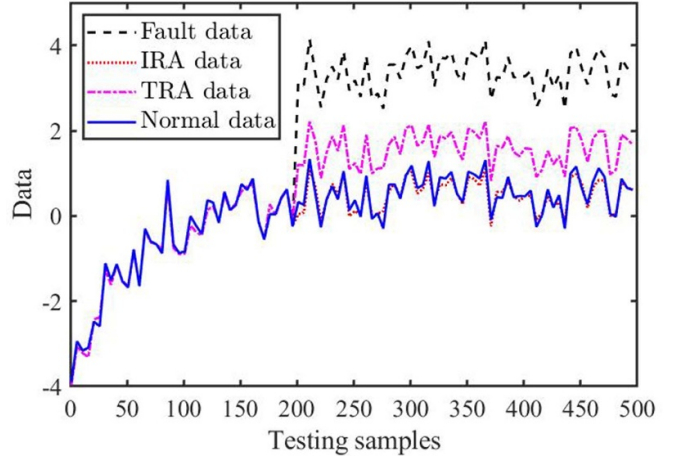


Figure 9. Reconstruction results of De_4 under the first scenario.

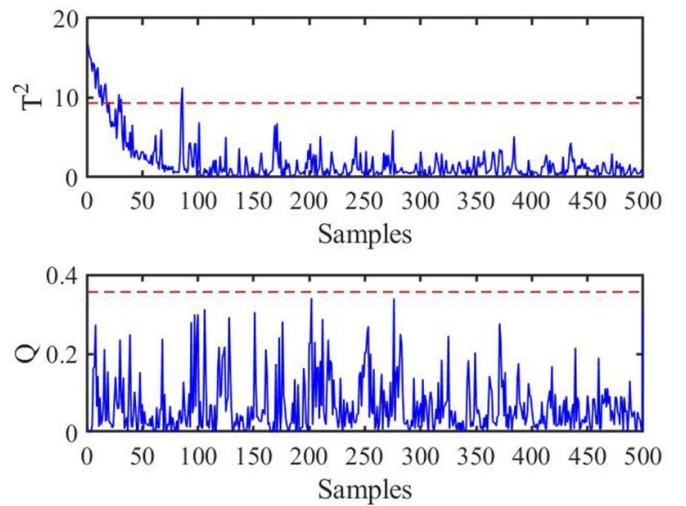


Figure 10. Results of third monitoring under the first scenario.

the third monitoring process is carried out. It can be observed from figure 10 that T^2 and Q statistics are below their control limits. Thus, all true faults are determined and the true fault set is $\{De_2 \& De_4\}$.

4.2. Scenario two: drift faults in sensor De_1 and De_2

In the second scenario, 0.3% and 0.6% drift faults are imposed on De_1 and De_2 (i.e. $C_2 = 0.3\%$ for De_1 , $C_2 = 0.6\%$ for De_2) at 5s, respectively. Figure 11 shows the responses of residual under this fault scenario. From the figure, the $CV = [1 \ 1 \ 1 \ 1 \ 1 \ 0 \ 0]$ is observed at $t = 5$ s. According to table 1, the PFS could be $\{De_1 \& De_2, Df_1 \& De_2, Df_1 \& De_1 \& De_2, Df_1 \& Df_2 \& De_2, Df_1 \& De_1 \& Df_2 \& De_2, De_1 \& Df_2 \& De_2\}$. In order to refine the PFS, Df_1 , De_1 , Df_2 and De_2 are monitored by the IPCA module. The first monitoring results are given in figure 12 where the faulty sensor De_2 is determined at the 212th sampling point. Thus, De_2 is

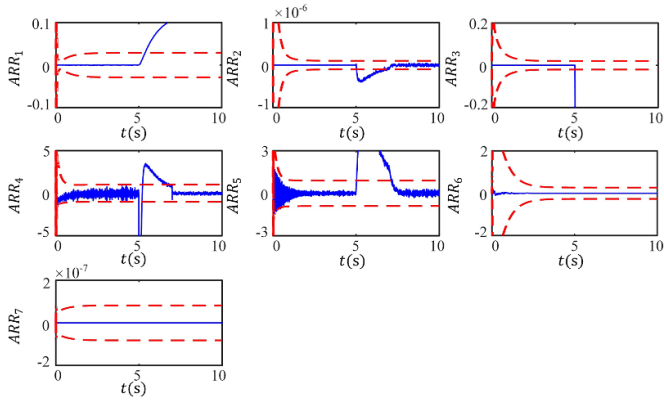
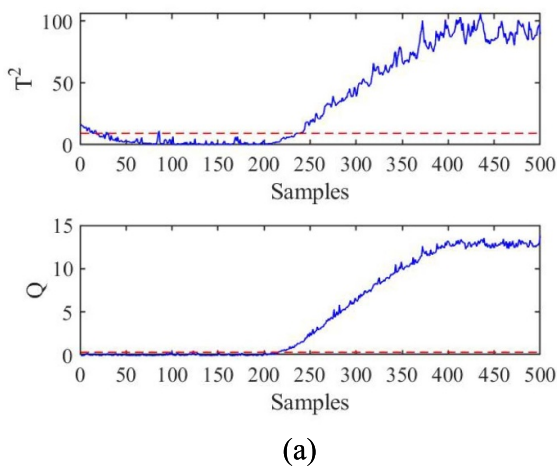


Figure 11. Residual responses under the second scenario.



(a)

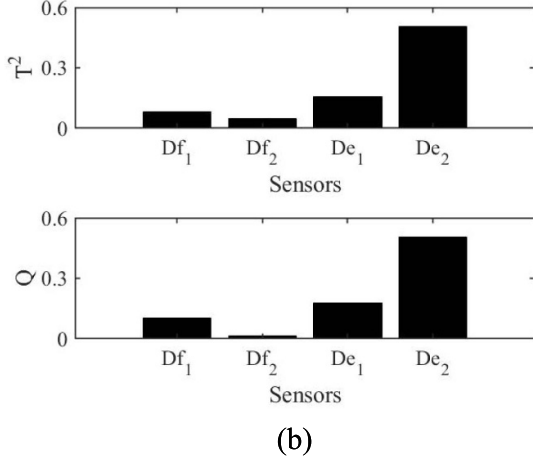


Figure 12. Results of first monitoring under the second scenario:
(a) T^2 and Q statistics; (b) contributions of possible faulty sensors to T^2 and Q statistics.

put into the true fault set and the fault reconstruction process is initiated at the 212th sampling point. Figure 13 shows the reconstruction results of De_2 based on IRA and TRA. It is found that the reconstructed data of TRA gradually deviate from the normal value of De_2 with the increase of time, while the reconstructed data of IRA is always consistent with the normal value. Thus, IRA can reconstruct the drift fault

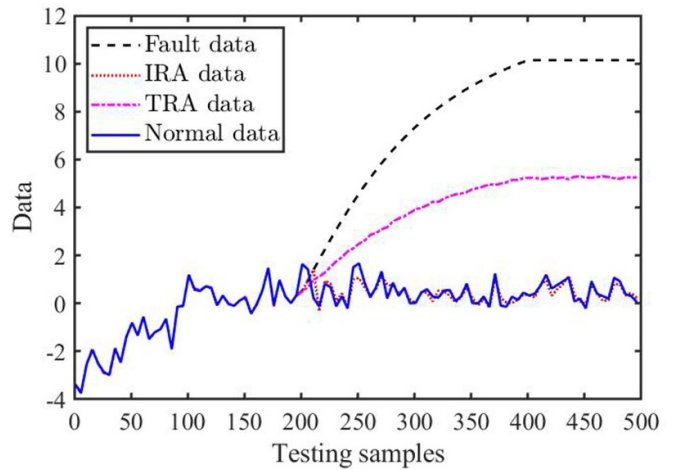
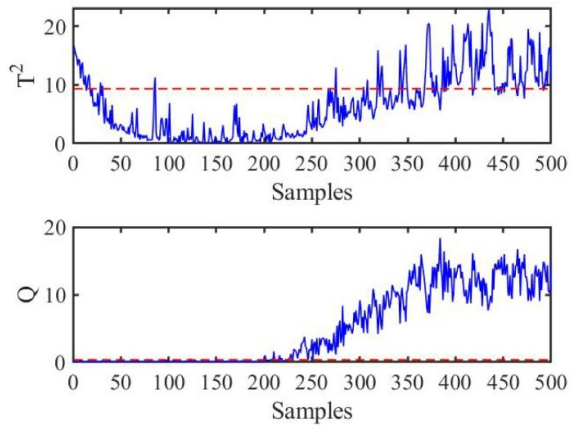


Figure 13. Reconstruction results of De_2 under the second scenario.



(a)

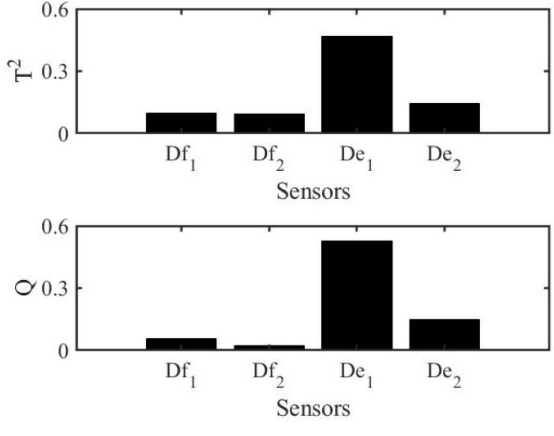


Figure 14. Results of second monitoring under the second scenario:
(a) T^2 and Q statistics; (b) contributions of possible faulty sensors to T^2 and Q statistics.

of sensor more accurately than TRA under multiple faults condition. After the fault data of De_2 are reconstructed by IRA, the second monitoring process is carried out. It can be

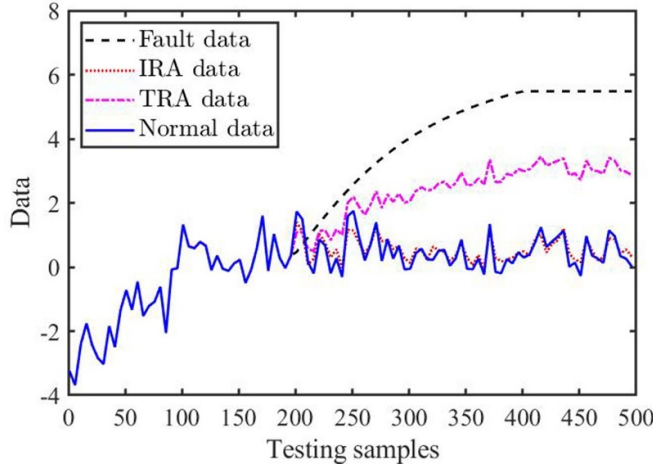


Figure 15. Reconstruction results of De_1 under the second scenario.

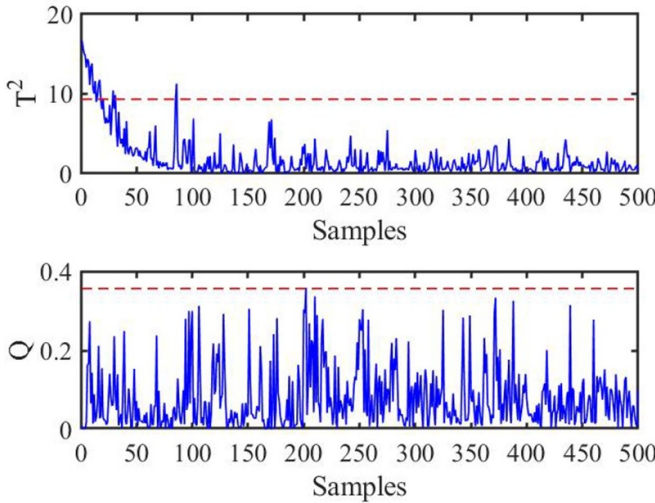


Figure 16. Results of third monitoring under the second scenario.

found from figure 14 that the faulty sensor De_1 is determined at the 205th sampling point. Therefore, De_1 is added to the true fault set. The reconstruction results of De_1 using IRA and TRA are given in figure 15. It is observed that the IRA successfully reconstructs the fault data of De_1 , but the TRA cannot function well. The reconstructed data of De_1 by IRA are employed instead of the fault data of De_1 , and the third monitoring process is enabled. As shown in figure 16, both T^2 and Q statistics stay within their control limits. Thus, the true faults are determined as $\{De_1 \& De_2\}$.

4.3. Scenario three: bias fault in Df_1 and drift fault in De_1

In this scenario, a 1% bias fault and 0.5% drift fault are introduced in Df_1 and De_1 (i.e. $C_1 = 1\%$ for Df_1 , $C_2 = 0.5\%$ for De_1) at $t = 5$ s, respectively. Figure 17 shows the residual responses under this fault scenario. After 5 s, the $CV = [1 \ 1 \ 1 \ 0 \ 0 \ 0 \ 0]$ is detected and the resulting PFS is $\{Df_1 \& De_1, De_1\}$. Therefore, Df_1 and De_1 are monitored by the IPCA module. The first monitoring results are illustrated in

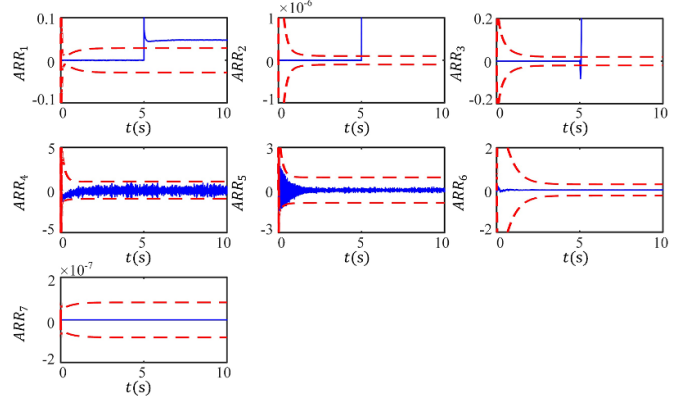


Figure 17. Residual responses under the third scenario.

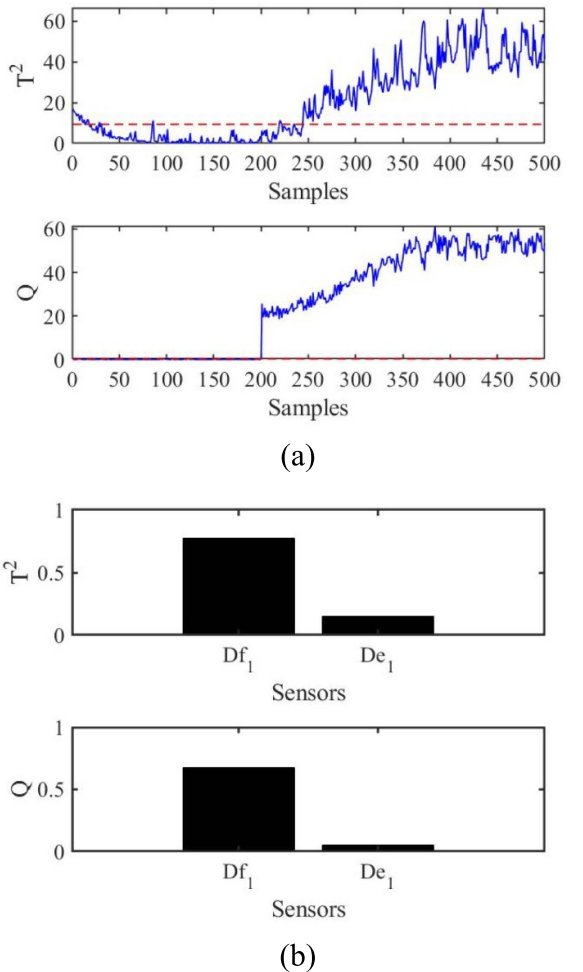


Figure 18. Results of first monitoring under the third scenario: (a) T^2 and Q statistics; (b) contributions of possible faulty sensors to T^2 and Q statistics.

figure 18 where the faulty sensor Df_1 is determined at the 200th sampling point. Based on the determined faulty sensor Df_1 and PFS (i.e. $\{Df_1 \& De_1, De_1\}$), the true fault set can be directly inferred as $\{Df_1 \& De_1\}$. In this scenario, the second monitoring process is not needed according to PFS, which reduces the computational cost of the algorithm.

5. Conclusions

In this paper, a new UBG-IPCA based sensor condition monitoring approach is developed for the dissimilar redundant actuation system of more electric aircraft. The effectiveness of the proposed approach is validated by simulation studies. The results of this work can be summarized as follows:

- (a) The UBG modeling technique is utilized to model the dissimilar redundant actuation system with uncertain parameters where the ARR_s and the adaptive thresholds are derived for fault detection and the FSM is established by the nominal parts of ARR_s for isolating the PFS. Various sensor faults can be considered due to the inherent symbolic structure of ARR_s.
- (b) The UBG-IPCA method is proposed for multiple faults isolation, where the IPCA module with the IRA and cyclic PCA monitoring model is introduced to further refine the PFS. The cyclic PCA monitoring model functions as the PCA monitoring module where the sensor with the maximum contribution to T^2 and Q statistics among all sensors is determined as a faulty sensor. The IRA algorithm is employed in the fault reconstruction module to reconstruct the data of a faulty sensor. In this way, the fault data of the sensor can be restored to the normal value, by which the fault characteristics can be eliminated.
- (c) According to the simulation results of three scenarios, it can be concluded that both the bias and drift faults of sensors can be handled by the UBG-IPCA method under the multiple faults condition. Compared with PCA, the computational cost of UBG-IPCA is less with the aid of PFS which can narrow down the scope of the fault isolation task. For example, in scenario three, the number of sensors monitored is decreased from seven to two. In addition, the proposed method does not need the information on fault type in advance.

In future work, there are three challenging issues to be addressed. First, since PCA is a linear dimensionality reduction method, the designed PCA cyclic monitoring model may not function well in nonlinear systems. Thus, a variety of nonlinear dimensionality reduction algorithms (such as kernel principle component analysis (KPCA) [27], t-distributed stochastic neighbor embedding (t-SNE) [28], locally linear embedding (LLE) [29], isometric mapping (ISOMAP) [30], etc) will be investigated for the nonlinear dissimilar redundant actuation system of more electric aircraft. Second, only the FDI method of the sensor is considered in this work. It is desirable to develop a remaining useful life prediction method in the faulty sensor for the dissimilar redundant system. Third, due to the limitations of experiment conditions, only simulation results are analyzed. In the future, the developed method will be applied to modern complex industrial systems with experimental validations to show practice significance.

Data availability statement

The data generated and/or analyzed during the current study are not publicly available for legal/ethical reasons but

are available from the corresponding author on reasonable request.

Acknowledgments

This research is supported by the National Natural Science Foundation of China (Grants Nos. 62173119 and 61673154).

ORCID iD

Ming Yu  <https://orcid.org/0000-0003-3703-9163>

References

- [1] Wang L and Mare J C 2014 A force equalization controller for active/active redundant actuation system involving servo-hydraulic and electro-mechanical technologies *Proc. Inst. Mech. Eng. G* **228** 1768–87
- [2] Wang J, Wang S, Wang X, Tomovic M M and Shi C 2018 Fault mode probability factor based fault-tolerant control for dissimilar redundant actuation system *Chin. J. Aeronaut.* **31** 965–75
- [3] Lu W, Teng J, Wen R, Zhu J and Li C 2017 Malfunction diagnosis of sensors based on correlation of measurements *Meas. Sci. Technol.* **28** 024004
- [4] Russell E L, Chiang L H and Braatz R D 2000 *Data-Driven Methods for Fault Detection and Diagnosis in Chemical Processes* (London: Springer)
- [5] Zhang D, Chen Y, Guo F, Karimi H R, Dong H and Xuan Q 2020 A new interpretable learning method for fault diagnosis of rolling bearings *IEEE Trans. Instrum. Meas.* **70** 3507010
- [6] Li W, Peng M and Wang Q 2019 Improved PCA method for sensor fault detection and isolation in a nuclear power plant *Nucl. Eng. Technol.* **51** 146–54
- [7] Bounouaa W and Bakdi A 2021 Fault detection and diagnosis of nonlinear dynamical processes through correlation dimension and fractal analysis based dynamic kernel PCA *Chem. Eng. Sci.* **229** 116099
- [8] Yu Y, Peng M, Wang H, Ma Z and Li W 2020 Improved PCA model for multiple fault detection, isolation and reconstruction of sensors in nuclear power plant *Ann. Nucl. Energy* **148** 107662
- [9] Xiao C, Yu M, Wang H, Zhang B and Wang D 2022 Prognosis of electric scooter with intermittent faults: dual degradation processes approach *IEEE Trans. Veh. Technol.* **71** 1411–25
- [10] Kumar P, Bensekrane I, Conrad B, Toguyeni A and Merzouki R 2019 Functionability analysis of redundant mechatronic systems in bond graph framework *IEEE/ASME Trans. Mechatronics* **24** 2465–76
- [11] Amirdehi S, Trajin B, Vidal P E, Vally J and Colin D 2020 Power transformer model in railway applications based on bond graph and parameter identification *IEEE Trans. Transp. Electrification* **6** 774–83
- [12] Venkatasubramanian V, Rengaswamy R, Yin K and Kavuri S N 2003 A review of process fault detection and diagnosis part I: quantitative model-based methods *Comput. Chem. Eng.* **27** 293–311
- [13] Lan D, Yu M, Huang Y, Ping Z and Zhang J 2022 Fault diagnosis and prognosis of steer-by-wire system based on finite state machine and extreme learning machine *Neural Comput. Appl.* **34** 5081–95
- [14] Levy R, Arogeti S, Wang D and Fivel O 2015 Improved diagnosis of hybrid systems using instantaneous sensitivity matrices *Mech. Mach. Theory* **91** 240–57

- [15] Yu M, Lan D, Jiang C, Xu B, Wang D and Zhu R 2022 Hybrid condition monitoring of nonlinear mechatronic system using biogeography-based optimization particle filter and optimized extreme learning machine *ISA Trans.* **120** 342–59
- [16] Said M, Fazai R, Abdellafou K B and Taouali O 2018 Decentralized fault detection and isolation using bond graph and PCA methods *Int. J. Adv. Manuf. Technol.* **99** 517–29
- [17] Yu M, Xiao C, Jiang W, Yang S and Wang H 2018 Fault diagnosis for electromechanical system via extended analytical redundancy relations *IEEE Trans. Ind. Inform.* **14** 5233–44
- [18] Mosadegh M, Jalili M M and Mazidi A 2011 Observability analysis for model-based fault detection and sensor selection in induction motors *Meas. Sci. Technol.* **22** 075202
- [19] Djeziri M A, Merzouki R, Bouamama B O and Dauphin-Tanguy G 2007 Robust fault diagnosis by using bond graph approach *IEEE/ASME Trans. Mechatronics* **12** 599–611
- [20] Samantaray A K, Medjaher K, Bouamama B O, Staroswiecki M and Dauphin-Tanguy G 2006 Diagnostic bond graphs for online fault detection and isolation *Simul. Modelling Pract. Theory* **14** 237–62
- [21] Valle S, Li W and Qin S J 1999 Selection of the number of principal components: the variance of the reconstruction error criterion with a comparison to other methods *Ind. Eng. Chem. Res.* **38** 4389–401
- [22] Bakdi A and Kouadri A 2017 A new adaptive PCA based thresholding scheme for fault detection in complex systems *Chemometr. Intell. Lab. Syst.* **162** 83–93
- [23] Alcala C F and Qin S J 2009 Reconstruction-based contribution for process monitoring *Automatica* **45** 1593–600
- [24] Waheed U R, Wang S, Wang X, Fan L and Kamran A S 2016 Motion synchronization in a dual redundant HA/EHA system by using a hybrid integrated intelligent control design *Chin. J. Aeronaut.* **29** 789–98
- [25] Fu J, Mare J C and Fu Y 2017 Modelling and simulation of flight control electromechanical actuators with special focus on model architecting *Chin. J. Aeronaut.* **30** 47–65
- [26] Chen Y and Lan L 2010 Fault detection, diagnosis and data recovery for a real building heating/cooling billing system *Energy Convers. Manage.* **51** 1015–24
- [27] Huang J and Yan X 2017 Quality relevant and independent two block monitoring based on mutual information and KPCA *IEEE Trans. Ind. Electron.* **64** 6518–27
- [28] Chatzimparmpas A, Martins R M and Kerren A 2020 t-viSNE: interactive assessment and interpretation of t-SNE projections *IEEE Trans. Vis. Comput. Graph.* **26** 2696–714
- [29] Liu H, Wang Z, Shang F, Yang S, Gou S and Jiao L 2018 Semi-supervised tensorial locally linear embedding for feature extraction using PolSAR data *IEEE J. Sel. Top. Signal Process.* **12** 1476–90
- [30] Zhang Z, Chow T W S and Zhao M 2013 M-isomap: orthogonal constrained marginal isomap for nonlinear dimensionality reduction *IEEE Trans. Cybern.* **43** 180–91